Journal of Theoretical and Applied Vibration and Acoustics 8(2) 1-20 (2022)

I S A V

Journal of Theoretical and Applied Vibration and Acoustics

journal homepage: http://tava.isav.ir

Detection of malfunction in ignition system for an internal combustion engine via artificial intelligence model

Mohammad Gohari [a,*], **Abbas Pak** [a], **Masoud Kazemi** [c]

[a] *Assistant Professor, School of Mechanical Engineering, Arak University of Technology, Arak, IRAN*

[b] *Assistant Professor, Department of Engineering, Bu-Ali Sina University, Hamedan, IRAN*

[c] *M.Sc. Student, School of Mechanical Engineering, Arak University of Technology, Arak, IRAN*

Research Article

ARTICLE INFO

Article history:
Received 12 June 2022

Received in revised form
30 July 2022

Accepted 9 September 2022

Available online 11 November 2022

Keywords:
Ignition system malfunction

Artificial intelligence model

Statistical features

Internal combustion engine

ABSTRACT

Engine failure is a significant issue for drivers, often requiring substantial experience to identify and troubleshoot effectively. Repairing the engine based on probable causes and uncertainties can be time-consuming and costly. Recently, AI models, particularly those based on Artificial Neural Networks (ANN), have been developed and gained popularity in fault diagnosis. This paper considers two common faults in internal combustion engines - cylinder misfire and complete cylinder failure - caused by ignition system issues. An Artificial Neural Network fed by Statistical features (SANN) is employed to distinguish these two faults. The SANN was trained on statistical features derived from vibration signals and achieved an accuracy of over 90%. Thus, SANN can classify the fault generated by the ignition system. This model was further validated using a different engine as a second case, demonstrating its ability to predict fault types with acceptable accuracy. In fact, the SANN could find a malfunction of the engine mounted on a car perfectly. This capability enables operators to accurately identify the type of fault, allowing for more precise and efficient repairs. Therefore, the proposed method is well-suited for troubleshooting ignition system malfunctions and diagnosing related issues via a reliable fault detection model.

1. Introduction

Diagnostic systems are employed in modern internal combustion engines (IC engines) to identify subsystems or engine components that are not functioning properly due to damage. Monitoring the engine's condition during operation can significantly reduce repair and maintenance costs by

* Corresponding author.
E-mail addres: moh-gohari@arakut.ac.ir (M. Gohari)

http://dx.doi.org/10.22064/tava.2024.555697.1206

enhancing durability and reliability. Fault detection techniques are continually evolving, with approaches including dynamical models, Fuzzy Logic (FL), ANN, and statistical models.

ANN models are inspired by the learning ability of the human brain. Similar to human learning, ANN methods can learn from examples. Essentially, ANNs use input-output sets to learn, adjusting internal node weights to minimize error in the output. As a result, ANNs are widely used for prediction, estimation, and pattern recognition, making them suitable for fault detection and classification. In the context of internal combustion engine fault detection, vibration signals from the engine block are typically processed using ANN techniques. The ANN can be fed with statistical features as input, or the vibration signal can first be decomposed using transforms such as Fourier or Wavelet. This hybrid approach enhances the performance of the ANN model and improves classification accuracy.

Despite significant advancements, the application of ANN in fault detection using vibration signals or acoustic emission methods remains an open area of research. For instance, Weidong Li et al. [1] investigated valve looseness monitoring using acoustic emission. In another study, Geng and Chen [2] analyzed piston slap vibration in IC engines, employing wavelet packets for signal decomposition. Shirazi and Mahjoob [3] used discrete wavelet transform (DWT) to convert the time-domain vibration signals of an IC engine into the time-frequency domain, achieving promising results in fault detection. Bao-Jia Chen et al. [4] utilized continuous wavelet transform (CWT) to feed an ANN for fault classification, achieving an efficiency of 100%. Junxing Hou et al. [5] studied knocking combustion in homogeneous charge compression ignition (HCCI) engines using wavelet packets. Additionally, Jian-Da Wu et al. integrated discrete wavelet packets (DWP) with ANN to detect faults such as injector malfunction and intake air deficiency in IC engines [6]. Nouri Khajavi et al. denoised vibration signals from an IC engine using wavelets, with signal energy serving as ANN input to detect faults like manifold absolute pressure sensor malfunctions, knock sensor issues, and misfires [7]. Furthermore, vibrational signal processing using DWT has been applied to analyze overhang slant cracked rotors [8]. Expert systems for fault detection based on wavelet analysis have also been proposed [9-11]. Beyond misfire detection, ANN-based vibration signal analysis has been utilized for other engine components, such as the timing belt and fuel ratio [12, 13]. Other hybrid techniques, including neuro-fuzzy approaches, have also been assessed for engine malfunction detection [14-21], or other fault detection and optimization by ANN [16, 22-24].

This paper aims to develop a model based on the vibration signals of an IC engine to detect faults in the electrical ignition system, such as misfiring and complete cylinder failure. The proposed ANN model is trained on statistical features extracted from engine block vibration signals. This model, referred to as SANN, is evaluated for its accuracy in fault classification, as discussed in the following sections.

2. Methodology

To develop a model for fault detection based on vibration data, a test rig setup and data acquisition system are required. In this investigation, vibration data are initially recorded from a standard engine operating without faults and an engine with faults in the ignition system. Subsequently, a gray box model was established based on the measured data. The gray box model's (SANN) performance was then evaluated and compared.

2.1. Data acquisition

A stationary four-stroke engine, identified as M13GS, is considered for indoor testing. The engine is mounted on a stand, and vibration data are gathered under normal operating conditions and with ignition system faults. The engine's rotational speeds are 1000, 2000, and 3000 RPM. Data collection is initiated when the engine's rotational speed is stable and maintained at the desired value.

2.2. Data acquisition equipment

The ADXL335 accelerometer records engine vibrations in three directions: X, Y, and Z. The Advantech-USB 4711A (Data Acquisition) system DAQ converts analog signals into digital signals and transmits them to a computer. The supply voltage for the transducer was set between 1.8 to 3.6V, with a current of 350 mA. The accelerometer is installed on the engine block, as shown in Figure 1. A low-pass filter is applied using LABVIEW software to eliminate the noise from the accelerometer's output signal. The data acquisition equipment and the engine mounted on the indoor stand are illustrated in Figure 2.

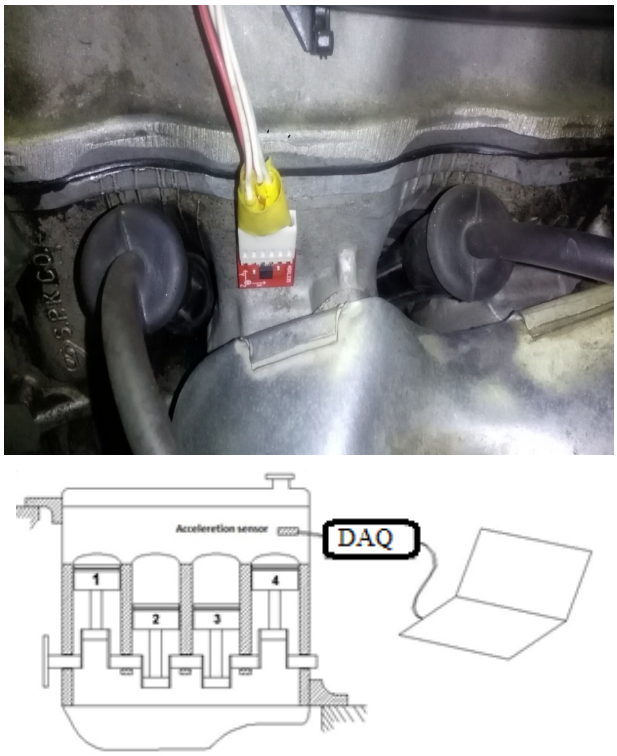

Fig. 1: The location of the accelerometer on the head of the engine block

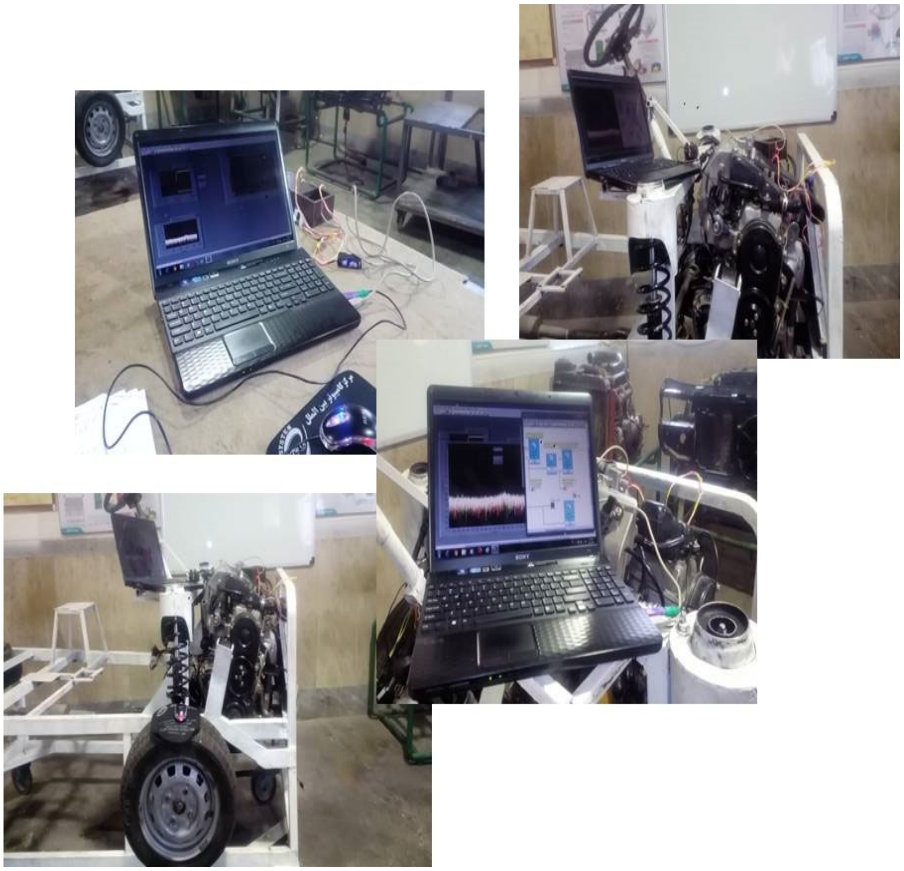

Fig. 2: Mounted engine on the stand and data collector equipment, including DAQ and a computer

The spark plug gap is adjusted to create three different combustion chamber conditions: misfire, no fire, and normal firing, as illustrated in Figure 3. As the spark plug gap increases by 20%, the required voltage for ignition rises by 99% [21]. Table 1 lists the spark plug gaps associated with normal firing and misfiring conditions.

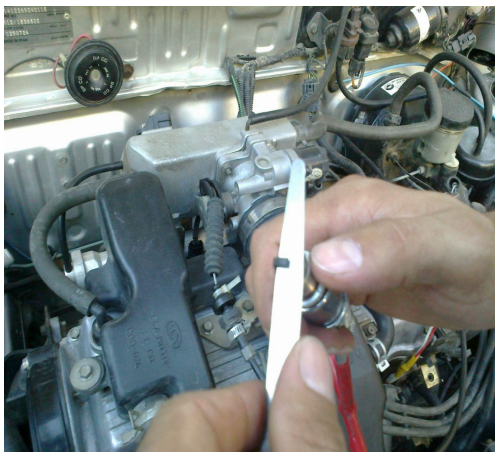

Fig. 3: Modifying the gap of the spark plug to make the fault

Table 1. Gap of spark plug

Gap of spark plug	Status of firing
0.750mm	Normal firing
0.90mm	Misfiring

Initially, tests are conducted with the engine running at a stable rotational speed of 1000 RPM, with each test repeated 9 times. These repetitions included scenarios of normal firing in all cylinders, misfiring, and no firing in the first, second, third, and fourth cylinders. The same tests are repeated at 2000 RPM and 3000 RPM. The engine's rotational speed is monitored using a diagnostic tool called Diag 2000. In total, 27 sets of vibrational data are collected from the engine block during these tests, as summarized in Table 2. The "MSF" shows which cylinder has a misfire fault, and the "WSP" illustrates the problem in the wire spark.

Table 2: Various test cases in normal firing, misfiring and no firing conditions.

Engine RPM	**Normal operation**	**Misfire in first cylinder**	**Misfire in second cylinder**	**Misfire in third cylinder**	**Misfire in fourth cylinder**	**No fire in first cylinder**	**No fire in second cylinder**	**No fire in third cylinder**	**No fire in fourth cylinder**
1000	N1	MSF1-A	MSF2-A	MSF3-A	MSF4-A	WSP1-A	WSP2-A	WSP3-A	**WSP4-A**
2000	N2	MSF1-B	MSF2-B	MSF3-B	MSF3-B	WSP1-B	WSP2-B	WSP3-B	**WSP4-B**
3000	N3	MSF1-C	MSF2-C	MSF3-C	MSF3-C	WSP1-C	WSP2-C	WSP3-C	**WSP4-C**

2.2. Noise filtering

The transducer initially records the acceleration signals in three directions (X, Y, Z) without any filtering, as shown in Figure 4. The figure reveals some variations in the raw signal that need to be removed. To address this, the Continuous Wavelet Transform (CWT) was employed to filter the signals. For example, the vibration signals in all three directions during normal firing at 2000 RPM are shown in Figure 5, while the signals during misfiring in the first cylinder at 1000, 2000, and 3000 RPM are depicted in Figure 6. Additionally, Figure 7 presents a sample of the Y-axis vibration signal with no firing in the third cylinder. An overview of the vibration signals across all three axes is provided in Figure 8.

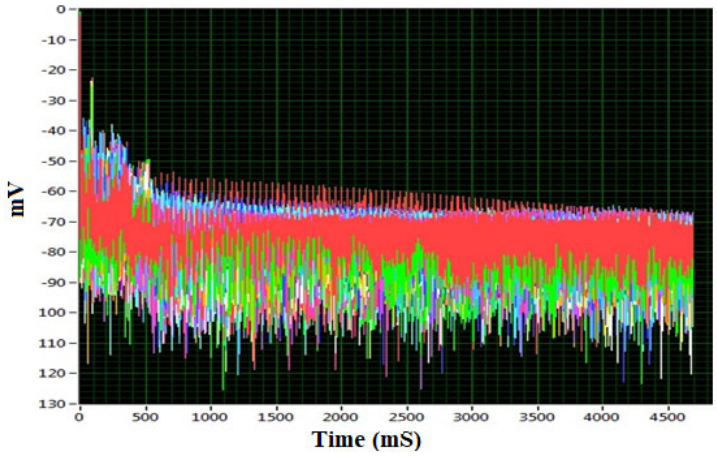

Fig. 4: The output voltage of accelerometer in three directions at 1000RPM

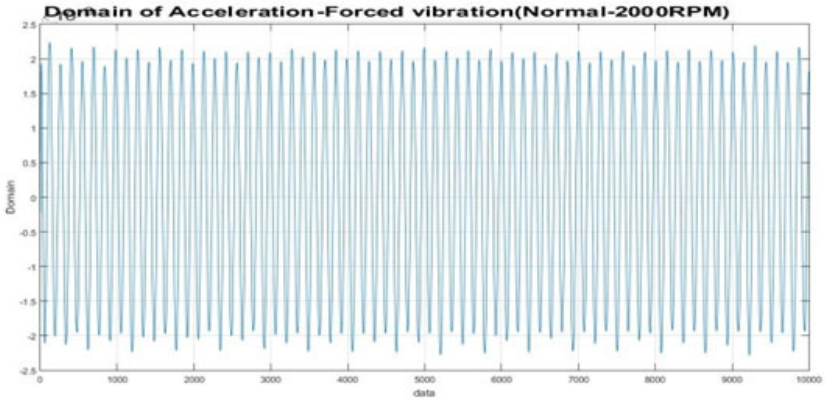

(a)

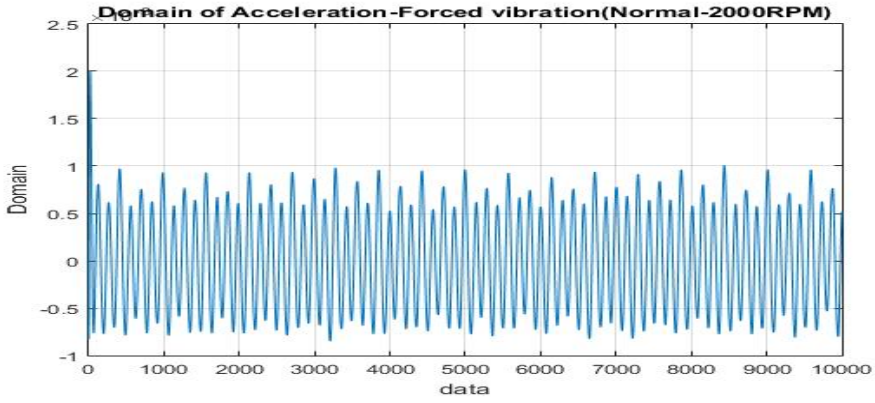

(b)

Fig. 5: Acceleration signals (m/s^2) in normal firing (2000RPM); (a) X-axis, (b) Y-axis, (c) Z-axis

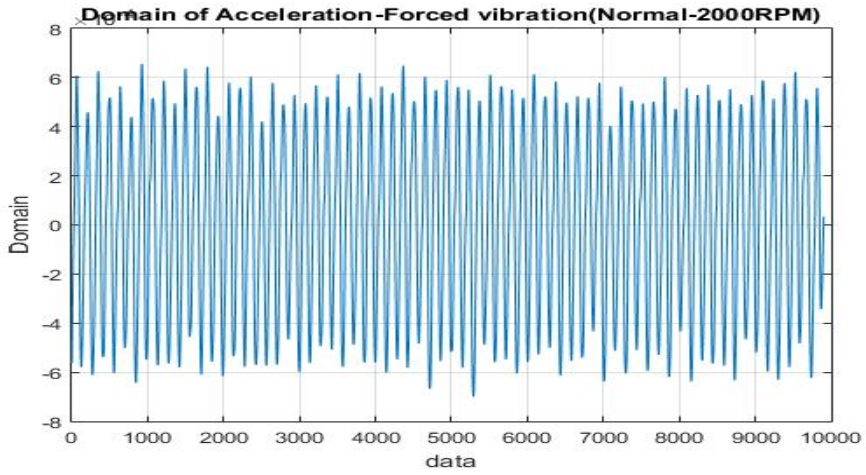

(c)

Fig. 5 (Cont.): Acceleration signals (m/s^2) in normal firing (2000RPM); (a) X-axis, (b) Y-axis, (c) Z-axis

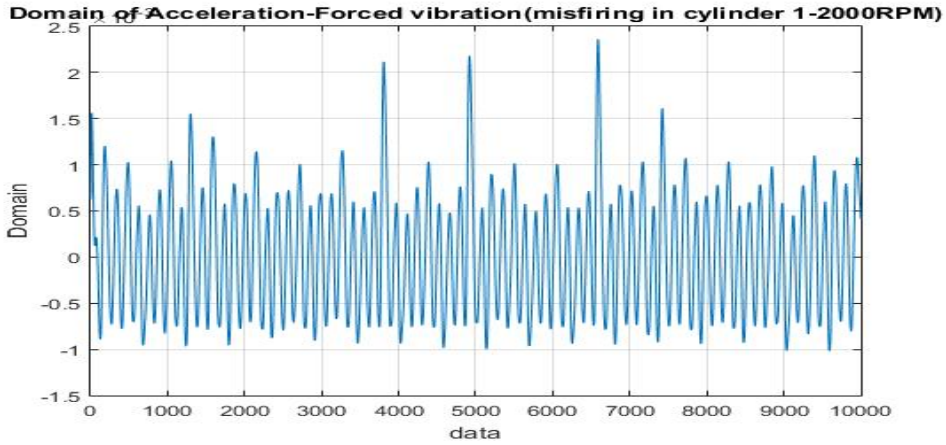

Fig. 6: Example signal of vibration in X-axis with misfiring in first cylinder (@ 2000 RPM)

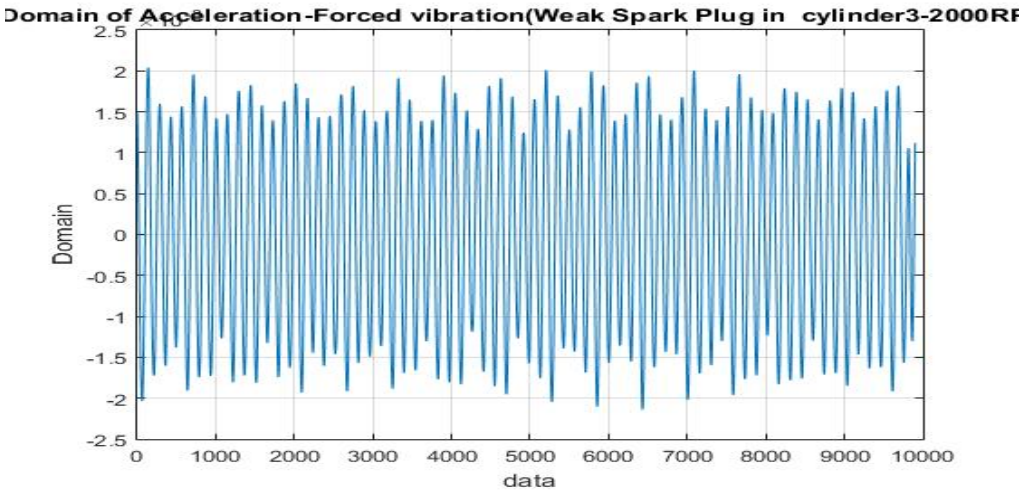

Fig. 7: Example of vibration signal in Y-axis with no firing in the third cylinder at 2000 RPM

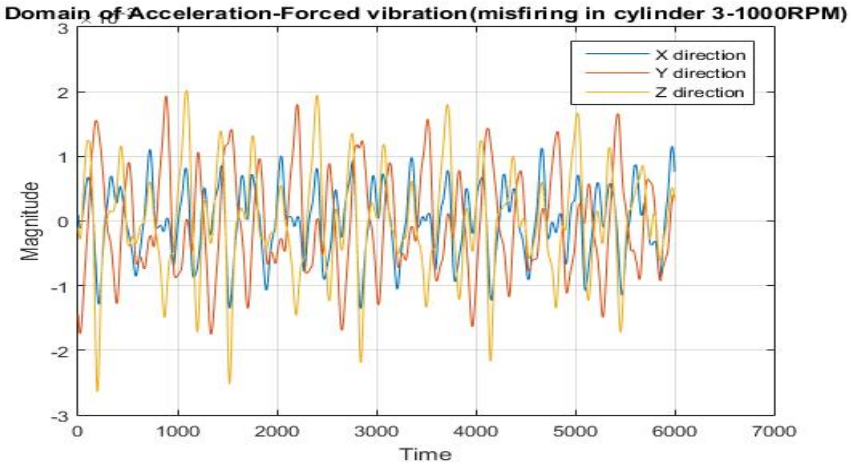

Fig. 8: Acceleration signal (m/s^2) in three axes with misfiring in the third cylinder at 1000RPM

3. Diagnosis model derivation

As previously discussed, this paper presents two AI models based on machine learning for fault detection in engines caused by issues within the ignition system. Figure 9 illustrates the proposed model called SANN. In this model, statistical features are extracted from time-domain acceleration signals and used as inputs for the ANN model. The following sections provide a detailed explanation of the components of the SANN model.

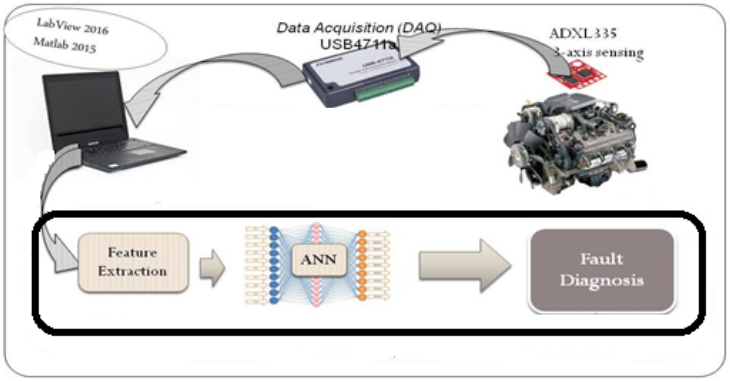

Fig. 9: Structure of SANN model in fault diagnosis

3.1. Proposed SANN model

Given that the recorded acceleration signals contain a large volume of complex data, using them directly as input signals would result in high CPU usage and significantly prolonged processing times. Therefore, a common approach is to extract statistical features that capture the primary behavior of the signals. The extracted features are listed and explained below:

- Root mean square (RMS)

The RMS can be calculated using the correlation given in Equation 1. Its value varies with vibrations.

$$\text{RMS} = \sqrt{\frac{1}{N} * \sum_{n=1}^{N} |x_n|^2} \tag{1}$$

where, X_n is acceleration data, and N is the number of data samples

- Crest Factor

This feature can be reached by dividing the peak value of the vibration signal by the RMS value:

$$\text{Crest Factor} = \frac{\mathbf{Max(x)}}{\mathbf{RMS}} \tag{2}$$

- Kurtosis Factor

This statistical parameter is helpful in machine fault detection at low speeds and discontinuing vibrations [22]. Normally, this value of the Kurtosis feature increases when the system is shocked by unpredicted fault. Kurtosis is calculated by:

$$\text{Kurtosis} = \frac{\mathbf{1}}{\mathbf{n}} * \left(\frac{\sum_{i=1}^{n}(x_i - u)}{\sigma}\right)^4 \tag{3}$$

- Impact Factor

Impact factor is a vital parameter in vibration analysis, and it is defined by dividing the peak of vibration by the average of data as follows:

$$\text{Impact Factor (IF)} = \frac{\mathbf{T_1}}{\frac{\mathbf{1}}{\mathbf{N}} * \sum_{\mathbf{n=1}}^{\mathbf{N}} |\mathbf{x(n)}|} \tag{4}$$

where, T_1 is the maximum value of recorded data.

- Standard Deviation

The standard deviation is an index of the distribution of data. In other words, a quantity that represents how far the members of a group differ from the mean value (T_2) for the group. The data with a standard deviation higher than 2 are typically removed due to invalidity.

$$\text{STD} = \sqrt{\frac{\sum_{n=1}^{N}[x(n) - T_2]^2}{N - 1}} \tag{5}$$

- Variance

Variance measures the spread between numbers in a data set and how far each member of the set is from the mean.

$$Var = \frac{\sum_{n=1}^{N}[x(n) - T_2]^2}{N - 1} \tag{6}$$

- Skewness

Skewness measures the asymmetry of the probability distribution of a real-valued random variable about its mean. It is the third standardized moment of a variable.

$$\text{Skewness} = \frac{\sum_{n=1}^{N}[x(n) - T_2]^3}{(N-1) * {T_3}^3} \tag{7}$$

where, T_3 is the standard deviation. Table 3 summarizes and labels all of the statistical features.

All ten statistical features are computed for the vertical vibrational signals using MATLAB software. In Table 4, the results of the calculation of the parameters are represented. As can be seen, by having misfire or no firing in the cylinders, the Skewness, Impact Factor, and Kurtosis vary drastically. On the other hand, for normal firing, the variation of stated features is not sensible. In addition, for better understanding, variations of the features are exhibited in Figures 10 and 11.

Table 3.: The statistical features applied in the SANN model

T1	$\max[\lvert x(n)\rvert]$	Maximum (x)	T6	$\frac{\sum_{n=1}^{N}[x(n)-T_2]^4}{(N-1)*{T_3}^4}$	Kurtosis (x)
T2	$\frac{\sum_{n=1}^{N}(x(n))}{N}$	Mean (x)	T7	$\frac{\sum_{n=1}^{N}\lvert x(n)\rvert}{N}$	Sum (abs(x))/N
T3	$\sqrt{\frac{\sum_{n=1}^{N}[x(n)-T_2]^2}{N-1}}$	Standard Deviation (x)	T8	$\frac{T_1}{\frac{1}{N}*\sum_{n=1}^{N}\lvert x(n)\rvert}$	Impact Factor (x)
T4	$\frac{\sum_{n=1}^{N}[x(n)-T_2]^2}{N-1}$	Variance (x)	T9	$\sqrt{\frac{1}{N}*\sum_{n=1}^{N}\lvert x_n\rvert^2}$	Root Means Square (RMS(x))
T5	$\frac{\sum_{n=1}^{N}[x(n)-T_2]^3}{(N-1)*{T_3}^3}$	Skewness (x)	T10	$\frac{N*\max[\lvert x(n)\rvert]}{T_1*\sum_{n=1}^{N}\lvert x(n)\rvert}$	Crest Factor

Table 4.: The statistical features derived from the vibrational signal at 1000 RPM

1000 rpm	Max	Std	Var	Skewness	Kurtosis	IF	RMS
N	0.1114246	0.0571241	0.00326283	0.150533913	1.6719838	2.19198107	0.057124054
MSF1	0.1680484	0.0622936	0.0038807	0.393965087	2.2314313	3.01910401	0.0622936
MSF2	0.1682269	0.0782395	0.00612173	0.374041305	2.3284672	3.02615654	0.07823954
MSF3	0.1747752	0.0702374	0.00493365	0.384334986	2.3700868	3.03355441	0.070237417
MSF4	0.1768462	0.0661389	0.00437446	0.246785339	2.3159653	3.09744573	0.066138851
WSP1	0.1173176	0.0641996	0.00412154	0.301124946	2.083945	2.56751998	0.064199647
WSP2	0.119115	0.0641738	0.00201552	0.276004411	2.0804901	2.90996473	0.064173821
WSP3	0.122566	0.0600788	0.00360953	0.293663343	2.2163851	2.94541918	0.060078766
WSP4	0.1283998	0.0642756	0.00668386	0.377784276	2.2871892	3.03147337	0.064275648

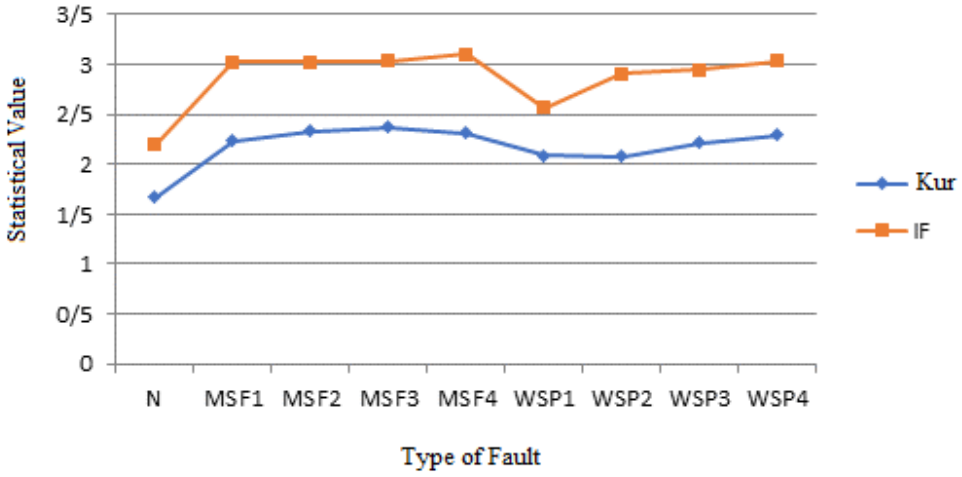

Fig. 10: Kurtosis and Impact Factor variations at 1000 RPM

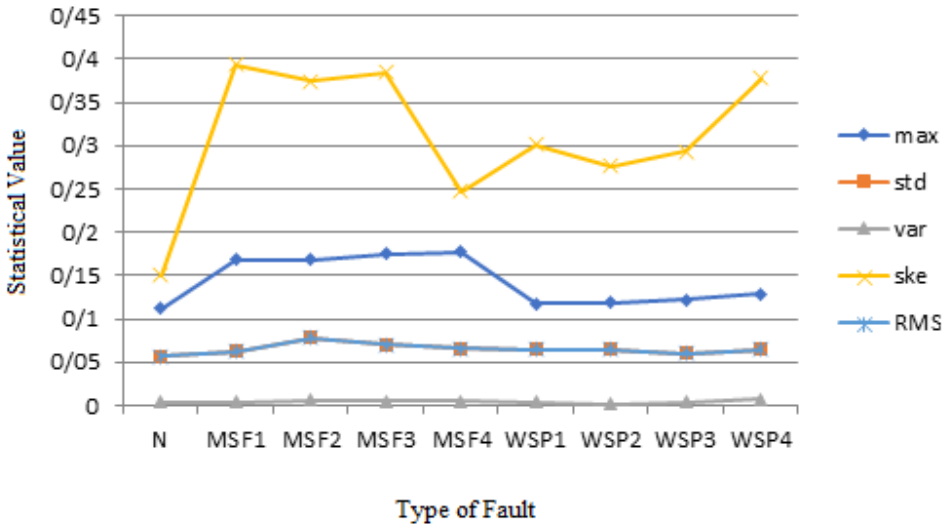

Fig. 11: Other statistical features differences at 1000 RPM

The statistical features have been calculated and described in Tables 5 and 6 for 2000 and 3000 RPM, respectively. Furthermore, the variations are revealed in Figures 12 to 15. Similar to the statistical features at 1000RPM, the Impact Factor, Skewness, and Kurtosis demonstrated severe differences.

Table 5: The statistical features derived from the vibrational signal at 2000 RPM

2000 rpm	Max	Std	Var	Skewness	Kurtosis	IF	RMS
N	0.19841523	0.130983	0.017157	-0.02426	1.514597	1.683999	0.130982
MSF1	0.23946912	0.15037	0.022611	-0.02416	1.591406	1.8787372	0.150364
MSF2	0.29188801	0.156694	0.024553	-0.01617	1.727686	2.1087657	0.156689
MSF3	0.27391242	0.150663	0.022699	-0.01795	1.729974	2.059421	0.150656
MSF4	0.29334877	0.168401	0.028359	-0.02107	1.617149	1.9554913	0.168402
WSP1	0.2160516	0.111835	0.012507	-0.02748	1.634501	1.9790828	0.111832
WSP2	0.21802402	0.102297	0.014459	-0.0235	1.631542	1.9837051	0.102292
WSP3	0.21882095	0.107081	0.011466	-0.01337	1.616841	1.9727983	0.107075
WSP4	0.22954195	0.142579	0.020329	-0.03485	1.538637	1.7932295	0.142572

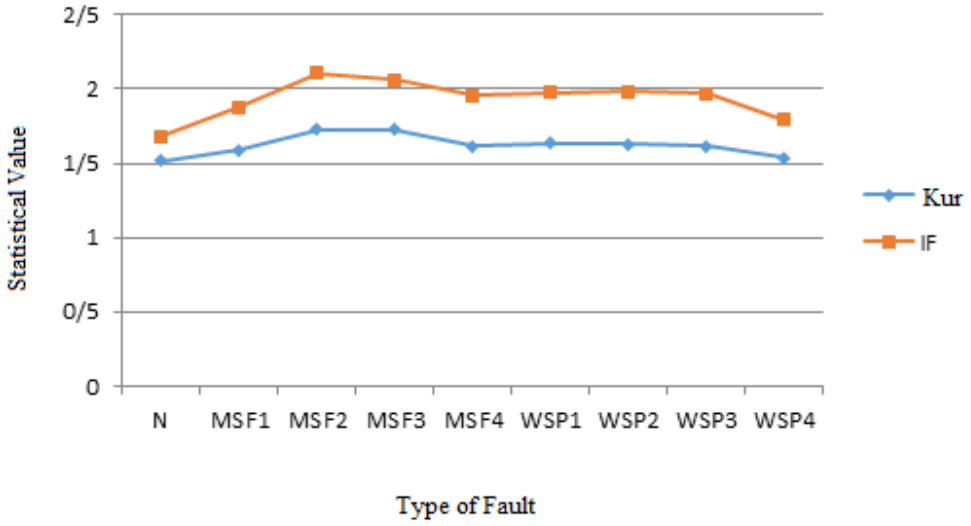

Fig. 12: The Kurtosis and Impact Factor Variations at 2000RPM

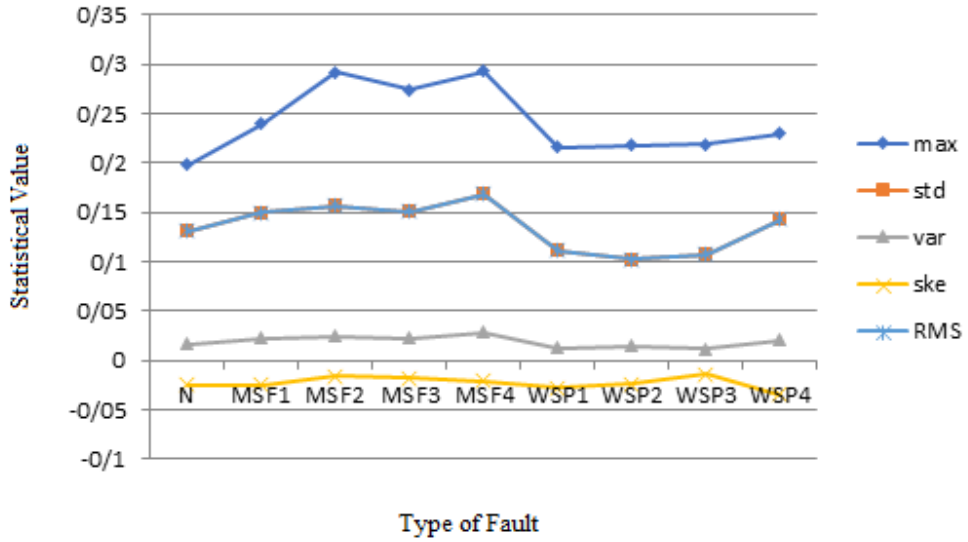

Fig. 13: Other statistical features differences at 2000 RPM

Table 6: The statistical features derived from the vibrational signal at 3000 RPM

3000 rpm	Max	Std	Var	Skewness	Kurtosis	IF	RMS
N	0.27866595	0.157092771	0.024678	0.012006	1.508853305	1.816715154	0.157092
MSF1	0.375669388	0.195668538	0.038286	0.006513	1.563299143	2.149017789	0.19566
MSF2	0.402060618	0.210431901	0.044282	0.028077	1.645509037	2.146887263	0.210421
MSF3	0.362127935	0.19522086	0.038111	-0.00131	1.650930747	2.087758202	0.195217
MSF4	0.388196257	0.206631078	0.042696	0.031511	1.596468578	2.103239189	0.206624
WSP1	0.309999667	0.177552611	0.031525	0.011922	1.525699341	1.917961524	0.17755
WSP2	0.328320766	0.185467727	0.010465	0.044336	1.604310323	1.98364301	0.185461
WSP3	0.332336461	0.18617133	0.03466	0.060456	1.560936526	1.99370936	0.186163
WSP4	0.328242217	0.194224577	0.037723	0.014871	1.541959589	1.883829804	0.194215

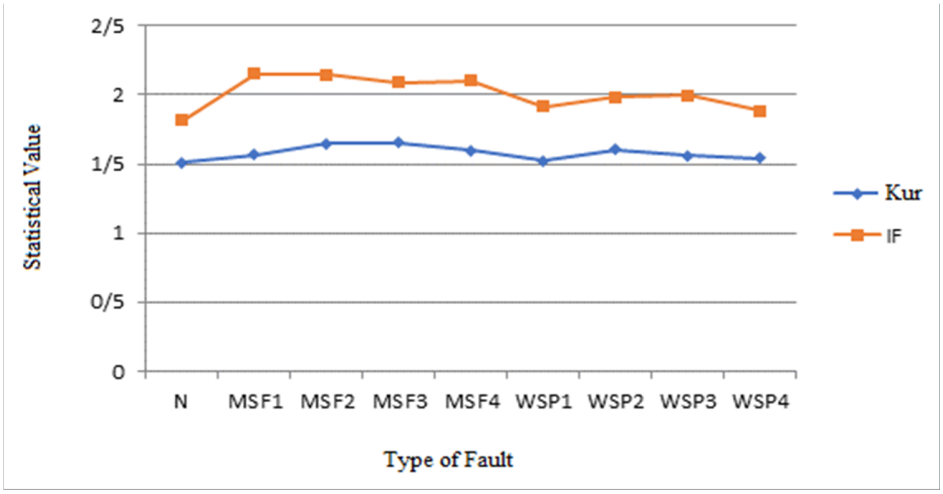

Fig. 14: The Kurtosis and Impact Factor variations at 3000RPM

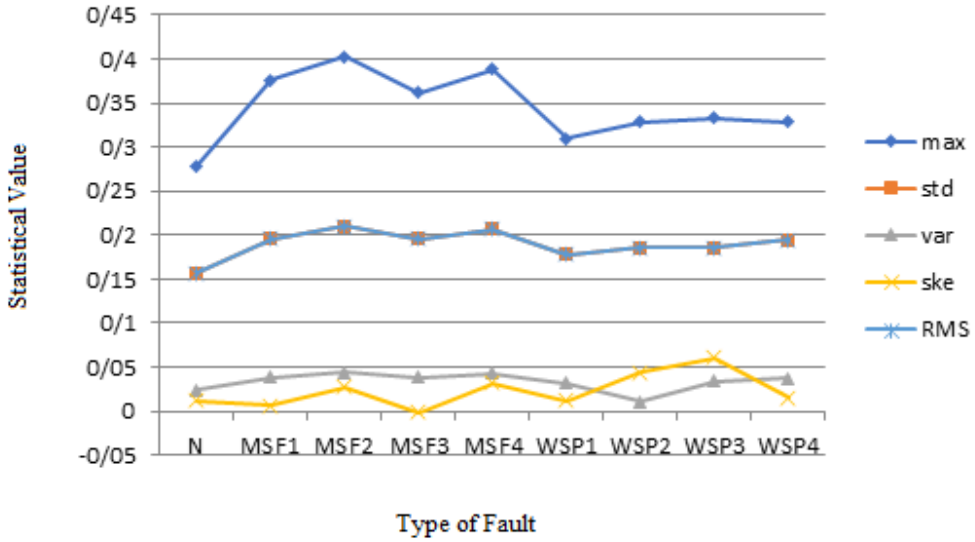

Fig. 15: Other statistical features differences at 3000 RPM

The statistical features are arranged in matrices as the inputs of the SANN model. The output matrix of the SANN model is encoded to show the class type of the engine faults. The target matrix presents a classification of the faults via a code. An example of an encoded target matrix is shown below:

1- Normal engine: [1 0 0 0 0 0 0 0 0]

2- Misfiring in the first cylinder: [0 0.2 0 0 0 0 0 0 0]

3- Misfiring in the second cylinder: [0 0 0.3 0 0 0 0 0 0]

4- Misfiring in the third cylinder: [0 0 0 0.4 0 0 0 0 0]

5- Misfiring in the fourth cylinder: [0 0 0 0 0.5 0 0 0 0]

6- No firing in the first cylinder: [0 0 0 0 0 1.6 0 0 0]

7- No firing in the second cylinder: [0 0 0 0 0 0 0.007 0 0]

8- No firing in the third cylinder: [0 0 0 0 0 0 0 1.8 0]

9- No firing in the fourth cylinder: [0 0 0 0 0 0 0 0 0.009]

In the case of a fault (misfire and no fire) in each cylinder, a number in a matrix with nine elements is considered. For example, the matrix of [1 0 0 0 0 0 0 0 0] is normal fire, but the matrix of [0 0.2 0 0 0 0 0 0 0] shows a misfire in the first cylinder. Also, [0 0 0 0 0 1.6 0 0 0] indicates no fire in the first cylinder. Actually, elements two to five correspond to misfire, and the last four correspond to no fire cases.

4. Results and discussions

Firstly, the topology and structure of SANN are presented, then the model's accuracy is discussed.

4.1. Topology of the SANN model

The SANN model includes an input layer, hidden layers, and an output layer. The input matrix contains the statistical features, and the target or the output layer consists of an encoded matrix based on the fault classification. In the training step, the Levenberg–Marquardt Algorithm (LM) is applied to learn the ANN. Different numbers of hidden layers are assessed, and the ANN model with 25 hidden layers presents the best efficiency. Seventy-five percent of data are used in the training step, and twenty-five percent are considered for validation and test steps. Figure 16 illustrates the topology of the SANN. Figure 17 exemplifies the performance of the Levenberg–Marquardt Algorithm versus the Scaled Conjugate Gradient Algorithm (SCG) during training. Likewise, over training has not happened in the network considering Figure 18.

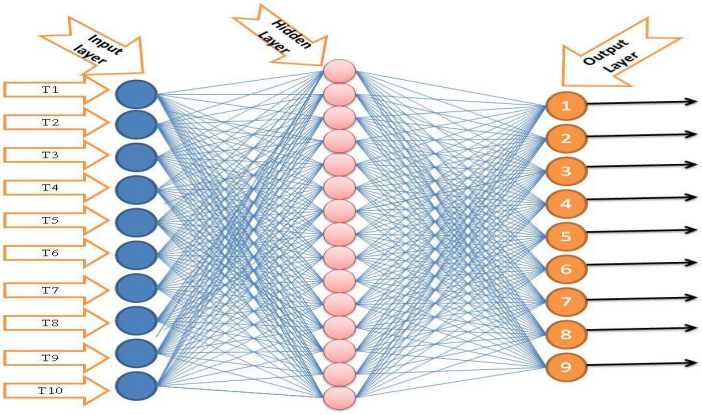

Fig. 16: Schematic topology of the SANN with the statistical features as inputs (T1 to T10)

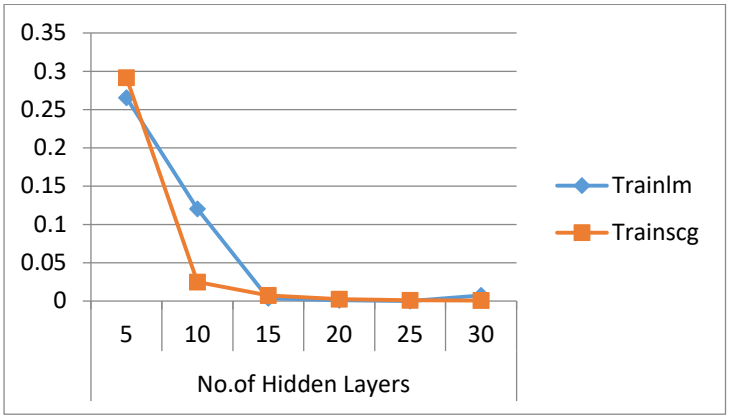

Fig. 17: Error of networks in prediction of output (LM Algorithm vs SCG Algorithm during training)

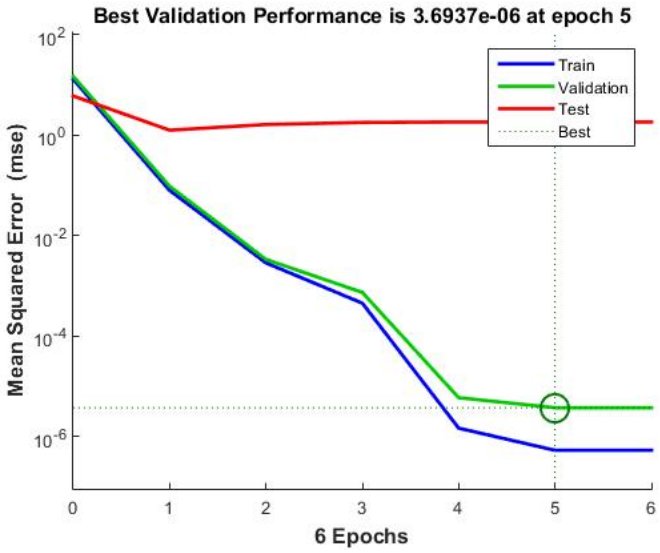

Fig. 18: Means Squared Error Vs Epoch

4.2. Accuracy of SANN

As can be seen in Figure 19, the overall correlation ratio is 0.99983, which shows the superior accuracy of the SANN Model in predicting engine faults in terms of misfiring or no fire in the combustion chamber.

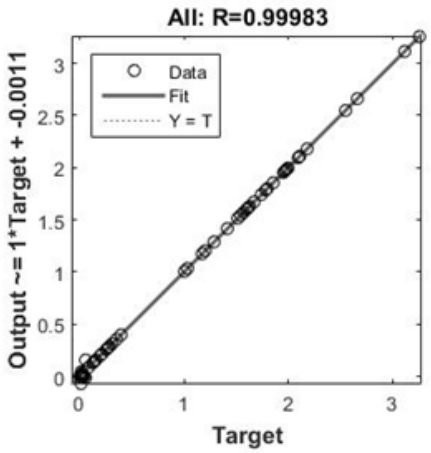

Fig. 19: The performance of SANN in Training, Validation, Test steps, and overall.

Another engine, mounted on a vehicle similar to the test rig engine, is tested to predict fault type in the cylinder. This additional study case is considered to assess the model performance. The results of this evaluation are shown in Figure 20. The prediction of Kurtosis via SANN is very close to actual type of faults. For example, normal firing that is the first point of the diagram is recognized by the SANN at 1000 RPM. The Second to fifth points show misfiring in one cylinder of the first to forth cylinder of engine block. The sixth point to tenth point illustrates no fire in one of the block cylinders. As shown in Figure 20, the convergence of actual fault type and diagnosed by SANN is superior, thus it can be employed for this purpose.

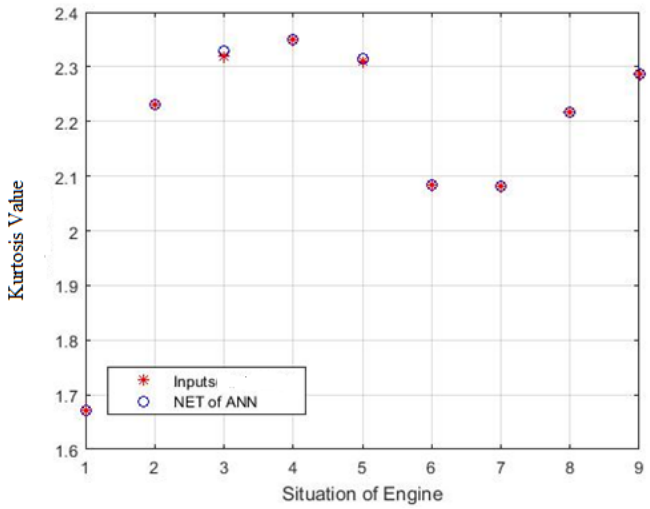

Fig. 20: The performance of SANN in fault diagnosis of the engine via perdition of the kurtosis value

5. Conclusion

AI models, particularly those based on ANN in fault diagnosis, have become popular in recent years. In This paper, two common faults of the internal combustion engine generated by the ignition system (no fire in a cylinder and misfire) are classified and detected by SANN, fed by statistical features derived from vibration signals. The accuracy of the SANN model is over 90%, and it was assessed by another engine working on the vehicle. The findings of this work may suggest that the SANN model can predict the type of fault with acceptable accuracy.

References

[1] W. Li, R.M. Parkin, J. Coy, F. Gu, Acoustic based condition monitoring of a diesel engine using self-organising map networks, Applied acoustics, 63 (2002) 699-711.
[2] Z. Geng, J. Chen, Investigation into piston-slap-induced vibration for engine condition simulation and monitoring, Journal of sound and vibration, 282 (2005) 735-751.
[3] F. Shirazi, M. Mahjoob, Application of discrete wavelet transform (DWT) in combustion failure detection of IC engines, in: 2007 5th International Symposium on Image and Signal Processing and Analysis, IEEE, 2007, pp. 482-486.
[4] B.-j. Chen, L. Li, X.-z. Zhao, Fault diagnosis method integrated on scale-wavelet power spectrum, rough set and neural network, in: 2007 International Conference on Wavelet Analysis and Pattern Recognition, IEEE, 2007, pp. 652-657.
[5] J. Hou, X. Qiao, Z. Wang, W. Liu, Z. Huang, Characterization of knocking combustion in HCCI DME engine using wavelet packet transform, Applied Energy, 87 (2010) 1239-1246.
[6] J.-D. Wu, C.-K. Huang, Y.-W. Chang, Y.-J. Shiao, Fault diagnosis for internal combustion engines using intake manifold pressure and artificial neural network, Expert Systems with Applications, 37 (2010) 949-958.
[7] M.N. Khajavi, S. Nasiri, A. Eslami, Combined fault detection and classification of internal combustion engine using neural network, Journal of Vibroengineering, 16 (2014) 3912-3921.
[8] Y.K. Maleki, M.S. Safizadeh, M.N. Khajavi, G. Payganeh, S. Shuruni, Over hang slant cracked rotor vibration signal processing based on discrete wavelet transform, in: 2016 13th International Multi-Conference on Systems, Signals & Devices (SSD), IEEE, 2016, pp. 672-676.
[9] J.-D. Wu, C.-H. Liu, An expert system for fault diagnosis in internal combustion engines using wavelet packet transform and neural network, Expert systems with applications, 36 (2009) 4278-4286.
[10] Y. Wang, N. Liu, H. Guo, X. Wang, An engine-fault-diagnosis system based on sound intensity analysis and wavelet packet pre-processing neural network, Engineering applications of artificial intelligence, 94 (2020) 103765.
[11] M. Hashim, M. Nasef, A. Kabeel, N.M. Ghazaly, Combustion fault detection technique of spark ignition engine based on wavelet packet transform and artificial neural network, Alexandria Engineering Journal, 59 (2020) 3687-3697.
[12] M. Khazaee, A. Banakar, B. Ghobadian, M.A. Mirsalim, S. Minaei, Remaining useful life (RUL) prediction of internal combustion engine timing belt based on vibration signals and artificial neural network, Neural Computing and Applications, 33 (2021) 7785-7801.
[13] M.H. Shahbaz, A.A. Amin, Design of active fault tolerant control system for air fuel ratio control of internal combustion engines using artificial neural networks, IEEE Access, 9 (2021) 46022-46032.

[14] L.A. Galiullin, R.A. Valiev, L.B. Mingaleeva, Development of a neuro-fuzzy diagnostic system mathematical model for internal combustion engines, HELIX, 8 (2018) 2535-2540.
[15] J. Gai, Y. Hu, Research on fault diagnosis based on singular value decomposition and fuzzy neural network, Shock and Vibration, 2018 (2018) 8218657.
[16] M. Gohari, R. Abd Rahman, R.I. Raja, M. Tahmasebi, Bus seat suspension modification for pregnant women, in: 2012 International Conference on Biomedical Engineering (ICoBE), IEEE, 2012, pp. 404-407.
[17] S. TayebiHaghighi, I. Koo, Sensor Fault Diagnosis Using an Indirect Fuzzy Feedback Linearization and Decision Trees, in: 2021 International Conference on Information and Communication Technology Convergence (ICTC), IEEE, 2021, pp. 1783-1788.
[18] J. Kang, Y. Lu, H. Luo, J. Li, Y. Hou, Y. Zhang, Wear assessment model for cylinder liner of internal combustion engine under fuzzy uncertainty, Mechanics & Industry, 22 (2021) 29.
[19] G. Macias-Bobadilla, J. Becerra-Ruiz, A.A. Estévez-Bén, J. Rodríguez-Reséndiz, Fuzzy control-based system feed-back by OBD-II data acquisition for complementary injection of hydrogen into internal combustion engines, International Journal of Hydrogen Energy, 45 (2020) 26604-26612.
[20] M. Montazeri-Gh, S. Yazdani, Application of interval type-2 fuzzy logic systems to gas turbine fault diagnosis, Applied Soft Computing, 96 (2020) 106703.
[21] S. Javan, S. Hosseini, S. Alaviyoun, F. Ommi, Effect of electrode erosion on the required ignition voltage of spark plug in CNG spark ignition engine, The Journal of Engine Research, 26 (2022) 31-39.
[22] S. Wadkar, Investigation for Distributed defects in Ball bearing using Vibration Signature Analysis-A Review.
[23] M. Gohari, A. Kord, Unbalance rotor parameters detection based on artificial neural network, Int J Acoust Vib, 24 (2019) 113-118.
[24] M. Gohari, A. Kord, H. Jalali, Unbalance rotor parameters detection based on artificial neural network: development of test rig, Journal of Vibration Engineering & Technologies, 10 (2022) 3147-3155.